Production of neutron-enriched isotopes along magic number $N = 126$ by multinucleon transfer reactions with radioactive-ion beams

V. V. Saiko [1,2,3,*] and A. V. Karpov [1,3,†]
[1] *Flerov Laboratory of Nuclear Reactions, JINR, 141980 Dubna, Russia*
[2] *Institute of Nuclear Physics, 050032 Almaty, Kazakhstan*
[3] *Dubna State University, 141982 Dubna, Russia*

(Received 25 March 2024; accepted 7 May 2024; published 6 June 2024)

Background: Multinucleon transfer (MNT) processes in low-energy deep inelastic (damped) collisions of heavy ions can be employed to produce heavy neutron-enriched nuclei. Recent progress in development of radioactive-ion beam (RIB) facilities may give additional possibilities in producing nuclei with large neutron excess.
Purpose: A major aim of the work is to calculate the cross sections of heavy neutron-rich isotopes with the magic number $N = 126$ in the reactions ^{132}Sn + ^{198}Pt and ^{136,138,140}Xe + ^{198}Pt within a multidimensional dynamical model based on the Langevin equations. Another purpose of the paper is to study the relative production rates of such nuclei reachable at currently working RIB facilities.
Method: A multidimensional dynamical model of nucleus-nucleus collisions based on the Langevin equations [A. V. Karpov and V. V. Saiko, Phys. Rev. C **96**, 024618 (2017)] has been used in the present work. This model provides a reasonable description of available experimental data.
Results: Cross sections of heavy neutron-enriched nuclides obtained in the MNT reactions ^{132}Sn + ^{198}Pt and ^{136,138,140}Xe + ^{198}Pt have been calculated. Relative production rates of these nuclei were estimated using beam intensities available at currently working RIB facilities.
Conclusions: Using neutron-rich radioactive projectiles in multinucleon transfer reactions with the ^{198}Pt target, one can reach an order of magnitude higher cross sections of neutron-enriched nuclides with the magic number $N = 126$. Relative production yields of such nuclei increase with the increasing N/Z ratio of the projectile.

DOI: 10.1103/PhysRevC.109.064607

I. INTRODUCTION

Throughout the history of nuclear physics research, more than 3000 nuclei have been explored. Most of them are nuclei with a proton excess, which are located to the left of the β-stability line on the map of nuclides. Although this region has been studied sufficiently well up to the proton drip line in a wide range of masses, in the area of neutron-rich nuclei there is a large number of yet unexplored nuclides, and the neutron drip line has been reached only for the light-mass region.

The fission and fragmentation reactions remain the main methods successfully utilized so far for the production of neutron-rich nuclei. A wide range of products from light to as heavy as uranium can be obtained in fragmentation of high-energy projectiles, while only medium-mass products can be formed in fission processes. Nowadays, the idea of using multinucleon transfer (MNT) reactions to synthesize neutron-rich nuclei is widely discussed [1–5]. Several dozens of neutron-rich nuclides have been identified exploring this type of reaction since it was discovered [6–10]. The main advantage of the multinucleon transfer mechanism is the wide range of isotopes produced near the colliding projectile and the target nuclei with quite high cross sections. However, at the same time, proper separation of the heavy nuclides from all MNT reaction products characterized by rather wide angular and energy distributions remains a challenging task.

An experimental study of properties and structure of neutron-rich nuclei is important, first of all, for a better understanding of the nuclear interaction. Measurement of lifetimes, masses, decay modes, and excited levels of new nuclei are of great value for testing and developing theoretical models of atomic nuclei. In addition, the properties of neutron-rich nuclei play a key role in understanding the detailed scenario of the r-process of astrophysical nucleosynthesis, which is one of the main sources of origin of chemical elements heavier than iron in the Universe. Special attention is paid to nuclei with a magic neutron number that form "waiting points" in the r-process path.

One of the least studied areas of neutron-rich nuclei that attracts the attention of researchers is the vicinity of the neutron shell closure $N = 126$. The most neutron-enriched isotope with the magic number $N = 126$ currently known is ^{202}Os, which was discovered in the fragmentation of uranium [11]. The experiment on the ^{136}Xe + ^{198}Pt reaction indicated that this nuclide can be produced in MNT processes with a rather higher cross section of ≈80 μb [12]. The possibility of synthesizing neutron-rich nuclei with $N = 126$ has

*saiko@jinr.ru
†karpov@jinr.ru

TABLE I. N/Z values of projectile and target for the studied reactions.

Reaction	$(N/Z)_p$	$(N/Z)_t$	$E_{c.m.}$ (MeV)
$^{136}Xe + ^{198}Pt$	1.519	1.538	498
$^{138}Xe + ^{198}Pt$	1.556	1.538	496
$^{140}Xe + ^{198}Pt$	1.593	1.538	495
$^{132}Sn + ^{198}Pt$	1.64	1.538	460

been analyzed in our previous article [2], where some of the promising combinations of heavy nuclei with the ^{136}Xe projectile were investigated within a multidimensional dynamical model based on Langevin equations. Reasonable agreement with available experimental data on angular, energy, mass, and charge distributions of MNT reaction products has been attained. In particular, our calculations indicated that the ^{198}Pt is probably the best target for reaching neutron-rich nuclei, being compared, i.e., with ^{208}Pb.

In this work, the production approach based on MNT reactions is extended by employing more neutron-enriched isotopes as projectiles [13]. In this case, one may expect even higher cross sections of nuclides with $N \approx 126$ than with the help of the stable ^{136}Xe projectile. It happens mainly due to the equilibration of the neutron-to-proton (N/Z) ratio that occurs in the early stage of heavy-ion collision and influences the direction of nucleon transfer [14]. In practice, the N/Z-equilibration process is only observed experimentally in collisions with neutron-deficient light projectiles, in which the N/Z ratio is less than that of the target (see, e.g., Refs. [15,16]). In this common case, proton stripping and neutron pickup processes dominate at the early stage of a collision [17,18]. In the opposite case, if the N/Z ratio of a projectile is higher than that of a target, the N/Z-equilibration process will predominantly proceed by neutron stripping and proton pickup (see Table I). Indeed, recent theoretical works confirm that the use of heavier isotopes of xenon as projectiles in MNT reactions leads to the production of heavy neutron-enriched nuclides near $N = 126$ with higher cross sections [19,20].

In practice, in this case we deal with unstable projectiles and hence with radioactive ion beams (RIBs), since ^{136}Xe is the heaviest stable isotope of xenon. Currently, there are several facilities around the world that can provide intensive RIBs of Xe isotopes, such as SPIRAL2 (GANIL), ISOLDE (CERN), FRIB (MSU), SPES (INFN), and ISAC (TRIUMF). The RIBs available in some of these facilities and their characteristics can be found in the corresponding Internet resources with open access [21–24]. In particular, the intensities of some radioactive Xe and Sn isotopes are shown in Fig. 1. One can see that the intensities of a given RIB obtained at all facilities have comparable values. More neutron-rich projectiles are produced with lower intensities as a result of a decrease in the cross section of their production in the fission process. Today, available RIB intensities are considerably lower than those provided for beams of stable isotope ^{136}Xe by approximately 2 orders of magnitude. However, considerable increase of intensities is expected in the near future with commissioning big RIB facilities of new generation, such as FAIR, EURISOL, and RAON, that are under construction now.

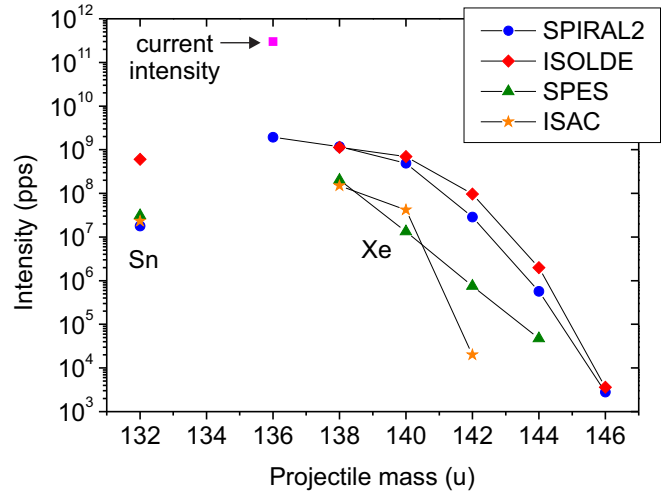

FIG. 1. Intensities of the radioactive beams of ^{132}Sn and heavy even-even Xe isotopes available at world-wide RIB facilities: SPIRAL2 of GANIL (circles) [21], ISOLDE of CERN (diamonds) [22], SPES of INFN (triangles) [23], and ISAC of TRIUMF (stars) [24]. The intensity of the primary proton beam of 2 μA was assumed in the case of the ISOLDE facility. The square indicates a current available intensity of the stable ^{136}Xe isotope.

Thus, on the one hand, employing RIBs in MNT reactions leads to an increase in cross sections, but on the other hand, their lower intensities reduce the final yield of products, which is proportional to the product of the cross section and the beam intensity. The purpose of this work is to study quantitatively the cross sections and the production rates of heavy neutron-rich isotopes with the magic number $N = 126$ in the MNT reactions ^{132}Sn + ^{198}Pt and ^{136,138,140}Xe + ^{198}Pt at comparable energies within the dynamical model based on the Langevin equations [2].

II. MODEL

The evolution of a collective degree of freedom in dissipative nuclear processes induced by heavy ions has the same stochastic nature as the motion of a Brownian particle in a liquid. On the basis of this analogy, a set of Langevin equations originally proposed to describe the Brownian motion is also applied in nuclear dynamics. The applicability of this approach to the description of nuclear dynamics is discussed in Refs. [25–27]. In particular, such processes as fusion, fission, quasifission, and deep inelastic scattering have been well described and understood using the dynamical approach based on Langevin equations [26,28–31]. The version of the dynamical model developed and refined in Refs. [2,32] is used in the present work. Here is only a brief description of the model.

In the model, a system of two colliding nuclei is described by 8 degrees of freedom. Four of them originate from the parametrization of the two-center shell model (TCSM) [33] and define the nuclear shape: distance r between geometrical centers of two nuclei, two independent ellipsoidal surface deformations $\delta_{1,2}$, and mass asymmetry $\eta_A = \frac{A_2 - A_1}{A_1 + A_2}$.

Furthermore, the charge asymmetry $\eta_Z = \frac{Z_2 - Z_1}{Z_1 + Z_2}$ defines the distribution of protons between fragments at fixed η_A. The angle θ between the internuclear axis and the beam direction, as well as the two rotation angles $\varphi_{1,2}$ of both fragments, are included in the model to evaluate their scattering angles and spins.

These degrees of freedom provide a continuous and smooth description of the nuclear shape of the system during a collision: two separated fragments at large distance and a composite dinuclear system after their contact. The time evolution of all degrees of freedom is defined by a set of eight coupled Langevin equations:

$$\dot{q}_i = \sum_j \mu_{ij} p_j,$$
$$\dot{p}_i = T\left(\frac{\partial S}{\partial q_i}\right)_{E_{\rm tot}} - \sum_{j,k} \gamma_{ij}\mu_{jk} p_k + \sum_j \theta_{ij}\xi_j(t), \quad (1)$$

where $q_i = \{r, \delta_1, \delta_2, \eta_A, \eta_Z, \theta, \varphi_1, \varphi_2\}$ and $p = \{p_r, p_{\delta_1}, p_{\delta_2}, p_{\eta_A}, p_{\eta_Z}, L, l_1, l_2\}$ are the collective degrees of freedom and their conjugate momenta, respectively. S and $T = \sqrt{E^*/a}$ are the entropy and temperature of the excited system, where a is the level density parameter and $E^* = E_{\rm tot} - V - E_{\rm kin}$ is the excitation energy. Here $E_{\rm tot}$ is the total energy of the system, $E_{\rm kin}$ is the kinetic energy stored in all collective degrees of freedom, and V is the potential energy. $\mu_{ij} = [m_{ij}]^{-1}$ is the inverse inertia tensor, γ_{ij} is the friction tensor, θ_{ij} are the amplitudes of the random force determined from the Einstein equation $\theta_{ik}\theta_{kj} = \gamma_{ij}T$, and ξ_i are normalized random variables with Gaussian distribution $\langle \xi_i(t) \rangle = 0$ and $\langle \xi_i(t), \xi_j(t') \rangle = 2\delta_{ij}\delta(t - t')$. The terms in Eq. (1) represent the driving, the friction, and the random forces, respectively. The driving force takes into account excitation of the nuclear system, while at $E^* \to 0$ it simplifies to $-\frac{\partial V}{\partial q_i}$.

The potential energy, friction, and inertia coefficients are the main values that govern the evolution of the nuclear system. We calculate them on a grid before starting the dynamical calculations. An extended macro-microscopic approach [34,35] based on the TCSM [33] is used to calculate the potential energy. The inertia coefficients for the collective degrees of freedom r, δ_1, δ_2, and η_A are calculated according to the Werner-Wheeler approach for an incompressible irrotational flow [36]. The corresponding friction coefficients are evaluated within the "wall + window" mechanism of one-body dissipation [37]. Inertia and friction coefficients for the charge asymmetry η_Z are calculated in the same way as in Ref. [27]. Compliance with the Pauli principle is taken into account in the calculations of the friction coefficients and the potential energy. The friction coefficients for angular degrees of freedom are estimated to be proportional to the radial friction coefficient γ_{rr} with the factor $K_{\rm tang}$. More details on the model and its parameters can be found in Refs. [2].

A set of Langevin equations (1) is solved numerically due to the presence of the random force. The colliding nuclei are set up at a distance of ≈50 fm with a fixed impact parameter, their surface deformations are defined by a minimum of potential energy, the mass and charge asymmetries correspond to initial values, and the deflection angle is defined analytically from the Coulomb trajectory. A projectile with a certain center-of-mass energy $E_{\rm c.m.}$ and with radial and angular momenta p_r and L approaches a target nucleus. In the case of a deformed colliding nucleus, it can be initially oriented by the tip or by the side toward the second nucleus. In the present work, the colliding nuclei ^{132}Sn, ^{136}Xe, ^{138}Xe, ^{140}Xe, and ^{198}Pt have nearly spherical shapes in the ground state, and the effects of mutual orientation can be neglected in the calculations.

Processes of nucleon transfer and dissipation of kinetic energy start to occur slightly before the nuclei come into contact. Then a composite dinuclear system is formed and evolved, finally decaying into two excited reaction fragments. The calculations are terminated when the formed binary products fly away reaching the initial distance. The later system evolution is again considered to proceed along a Coulomb trajectory. Thus, the obtained unique multidimensional trajectory provides all characteristics of a collision and primary products, such as nucleon numbers, scattering angles, kinetic and excitation energies, etc. We simulate an ensemble of such random trajectories for each impact parameter of a valuable range $0 < b < b_{\rm max}$ in order to explore the variety of exit channels in heavy-ion collisions.

The deexcitation process of primary products is treated within the statistical model [2,38]. It requires excitation energy and spin of products as input data. Dynamical calculations provide the spins of the fragments and the total excitation energy of the system. The last value is divided between fragments proportionally to their masses.

In the present work, Monte Carlo simulation of the decay cascade is performed separately for each primary excited product. The evaporation of neutrons, protons, α particles, and γ quanta as well as the sequential fission process, are considered at each step of the decay cascade. The evaporation of light particles or γ quanta reduces the excitation energy and spin of the fragment. The decay cascade terminated when either the fission occurred or the excitation energy was completely consumed and the evaporation residue was formed. In the former case, the masses of sequential fission fragments are simulated using the GEF code [39], their total kinetic energy is defined according to systematics [40], and isotropic emission in the center-of-mass system of the fissioning nucleus is assumed. Thus, we obtain information on the final reaction products that allows us to compare the distributions consistently with the experimental data.

Finally, differential cross sections are calculated as

$$\frac{d^4\sigma}{dZdAdEd\Omega}(Z, A, E, \theta) = \int_0^{b_{\rm max}} \frac{\Delta N(b, Z, A, E, \theta)}{N_{\rm tot}(b)} \frac{b\,db}{\Delta Z \Delta A \Delta E \sin\theta \Delta\theta}, \quad (2)$$

where ΔN is the number of trajectories in a given bin and $N_{\rm tot}$ is the total number of simulated trajectories for each impact parameter. Integration of Eq. (2) allows one to obtain different distributions of reaction products.

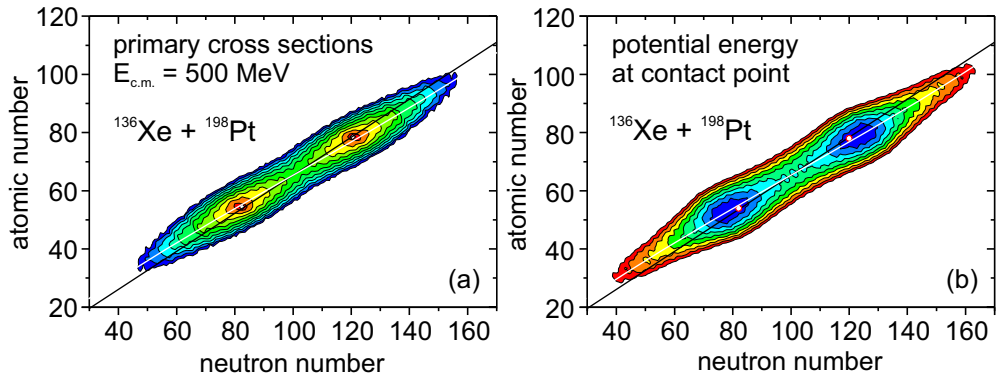

FIG. 2. (a) The N-Z distribution of primary products of the $^{136}\mathrm{Xe} + {}^{198}\mathrm{Pt}$ reaction calculated at $E_{\mathrm{c.m.}} = 498$ MeV. Cross sections are presented in logarithmic scale, and contour lines are plotted over half of an order of magnitude starting from 1 μb. (b) Potential energy landscape of the $^{136}\mathrm{Xe} + {}^{198}\mathrm{Pt}$ system in the N-Z plane calculated at the contact point assuming spherical shapes of the fragments. Contour lines are drawn over 10 MeV. Open circles indicate the projectile and the target nuclei. The black line and the white curve in both panels indicate the Z/N ratio of the composite system and the bottom of the potential energy landscape, respectively.

III. RESULTS

A. Primary cross sections

We have analyzed multinucleon transfer processes occurring in the $^{132}\mathrm{Sn} + {}^{198}\mathrm{Pt}$ and $^{136,138,140}\mathrm{Xe} + {}^{198}\mathrm{Pt}$ reactions at energies 460, 498, 496, and 495 MeV in the center-of-mass system, respectively. These energy values are 20% higher than the corresponding Bass barrier V_B [41]. Many excited nuclides are produced near the projectile and the target as a result of these MNT reactions. The variety of primary products obtained in these reactions can be conveniently shown as a two-dimensional distribution in the N-Z plane. This distribution plotted for the case of the $^{136}\mathrm{Xe} + {}^{198}\mathrm{Pt}$ reaction in the logarithmic scale is shown in Fig. 2(a). The shape of the distribution is elongated along the nuclei with nearly the same N/Z ratio as the one of the composite system $N_{\mathrm{tot}}/Z_{\mathrm{tot}}$, which is in accordance with the potential energy surface of the system shown in Fig. 2(b). This landscape of the potential energy has been calculated at the contact point of the $^{136}\mathrm{Xe} + {}^{198}\mathrm{Pt}$ system in the N-Z plane. The spherical shapes of both fragments have been assumed in the calculation.

The minimum of the potential energy landscape in the N-Z plane indicated by the white curve in Fig. 2(b) slightly deviates from the assumption of uniform charge distribution indicated by the straight black line. This happens because the heavier the fragment is the more neutrons it must contain to compensate for the Coulomb repulsion of its protons. Thus, the minimal Q value is achieved when the N/Z ratio of a heavy fragment is slightly higher than that of a light one.

The white curve [same meaning as in Fig. 2(b)] is also shown in Fig. 2(a). It can be seen that the cross-section distribution is elongated just along the minimum of the potential energy in the N-Z plane. Thus, we can estimate the most probable N/Z ratio of the primary MNT products obtained in the reactions under study by analyzing such potential energy surfaces illustrated in Figs. 3(a)–3(d). Calculations were made for the configuration of two touching spherical nuclei as in Fig. 2(b) and the results for the region of targetlike fragments (TLFs) are shown.

The $^{136}\mathrm{Xe} + {}^{198}\mathrm{Pt}$ system is initially in a state with the potential energy close to a minimum [Fig. 3(a)]. All other systems consisting of a projectile with the N/Z ratios higher than that of the target are initially located on the side wall of the potential energy valley. Thus, they experience a driving force that tends to put them to the bottom of the valley shown by the white curve in Fig. 3. The higher the N/Z ratio of the projectile is the further the bottom line of the potential energy will extend from the target nucleus to the region of more neutron-enriched heavy fragments.

The cross sections of the primary TLFs obtained in the reactions under study are shown in Figs. 3(e)–3(h). Formation of neutron-rich TLFs with N/Z ratios corresponding to the minimum of the potential energy with high cross sections is observed in all the cases. The transfer of neutrons from the projectile to the target (neutron stripping) and the transfer of protons in the reverse direction (proton pickup) become dominant in these reactions [see Figs. 3(g) and 3(h)]. Such cross-exchange of protons and neutrons due to different N/Z ratios of colliding nuclei is the main mechanism of the N/Z equilibration process, which leads to the formation of TLFs with larger neutron excess in the MNT processes.

Actually, the landscape of potential energy is very sensitive to the fragment deformations. This is the reason why the directions of the potential energy gradient shown by the arrows in Figs. 3(a)–3(d) may not coincide with the direction of predominant nucleon flow traced in cross sections of primary fragments (for example, the $^{140}\mathrm{Xe} + {}^{198}\mathrm{Pt}$ system).

Thus, the N/Z equilibration process in the $^{140}\mathrm{Xe} + {}^{198}\mathrm{Pt}$ and $^{132}\mathrm{Sn} + {}^{198}\mathrm{Pt}$ reactions leads to the formation of more neutron-rich isotopes of elements lighter than the target at an early stage of the reaction, which increases the probability of reaching the region of unknown nuclei near the $N = 126$ neutron shell closure.

Excited fragments formed in these MNT processes evaporate light particles, predominantly neutrons, and can decay by sequential fission. Thus, simulation of the decay cascade of primary fragments within the statistical model allows us to obtain cross sections of the final fragments.

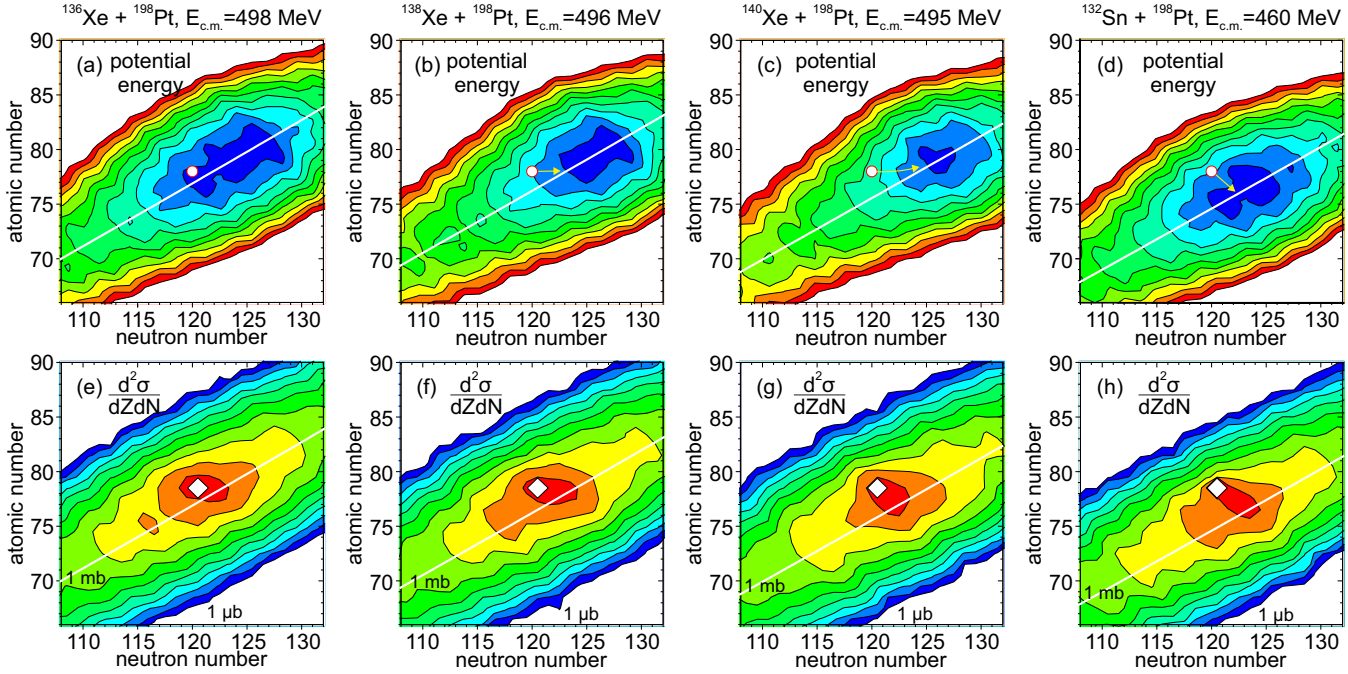

FIG. 3. (a)–(d) The potential energy landscape near the target nucleus ^{198}Pt in the N-Z plane calculated for the ^{136}Xe + ^{198}Pt, ^{138}Xe + ^{198}Pt, ^{140}Xe + ^{198}Pt, and ^{132}Sn + ^{198}Pt systems at the contact point assuming spherical shapes of fragments. Contour lines are drawn over 5 MeV. Open circles indicate the target nucleus. (e)–(h) The N-Z distribution of the primary targetlike products obtained in the corresponding reactions. Cross sections are presented in logarithmic scale as in Fig. 2. The white curve in all panels indicates the bottom of the potential energy landscape.

B. Final cross sections

The experimental identification of such heavy fragments like those near the $N = 126$ shell closure produced in MNT reactions is a complicated and challenging task. The dE-E and time-of-flight methods, as well as magnetic spectrometers, are usually applied to measure the atomic number and/or the mass of light PLFs. However, these methods are not applicable for the unambiguous identification of heavy TLFs. Radiochemical and spectroscopic methods are conventionally used for this purpose.

Recently, the ^{136}Xe + ^{198}Pt reaction was investigated at the energy $E_{\text{c.m.}} = 450$ MeV within the Gammasphere setup [42]. Both light and heavy reaction products were identified by γ-decay chains during irradiation. This method was used to obtain information about stable and short-lived nuclides. The analysis of γ decays after irradiation of the target made it possible to determine the long-lived reaction products. The measured isotopic distributions of the TLFs produced in this experiment are shown in Fig. 4. Results of the calculation carried out within the present dynamical model (labeled as "Langevin") and the theoretical approaches ImQMD [43], DNS [19], and GRAZING-F [44] are also illustrated in Fig. 4 by histograms.

Channels with transfer of up to seven protons are observed in this reaction. The results of calculations of the dynamical model are generally consistent with the experimental data, indicating rather wide and high isotopic distributions. However, the Langevin-type dynamical model overestimates the production cross sections of the neutron-enriched isotopes of chemical elements heavier than the target [Figs. 4(j)–4(n)]. Rather close results were obtained within the framework of the improved quantum molecular dynamics (ImQMD) approach.

Similar behavior was observed in the analysis of the experimental data obtained in the ^{136}Xe + ^{208}Pb reaction, which was measured at the energy $E_{\text{c.m.}} = 450$ MeV using the same technique (see Fig. 15 in Ref. [2]).

In the present work, we are interested in the cross sections of neutron-enriched isotopes of elements lighter than the target obtained in the ^{136}Xe + ^{198}Pt and similar reactions. Figure 4 illustrates that there is a lack of experimental data for such products and, therefore, it is difficult to estimate reliability of the model predictions in this region. However, the dynamical model describes very well the distributions of the Os and Hg isotopes obtained in the measurements of the ^{136}Xe + ^{198}Pt reaction at energy $E_{\text{c.m.}} = 643$ MeV [12] (see Fig. 18 in Ref. [2]).

Reasonable overall description of the experimental data on the ^{136}Xe + ^{198}Pt reaction demonstrated in this section and in Ref. [2] supports the present analysis of MNT processes that occurred in similar reactions with the same target ^{198}Pt.

The results of the calculations carried out in the framework of the dynamical model for the MNT reactions of the ^{198}Pt target with the ^{138,140}Xe and ^{132}Sn radioactive beams are shown in Fig. 5. Using the more neutron-enriched projectiles, one can produce the neutron-enriched nuclides with the higher cross sections. The ^{132}Sn projectile is more efficient than the ^{140}Xe one because of the higher N/Z ratio (see Table I). The region of yet unknown neutron-enriched isotopes delimited by dashed vertical lines in Fig. 5 can be reached in such reactions for chemical elements lighter than platinum with rather high

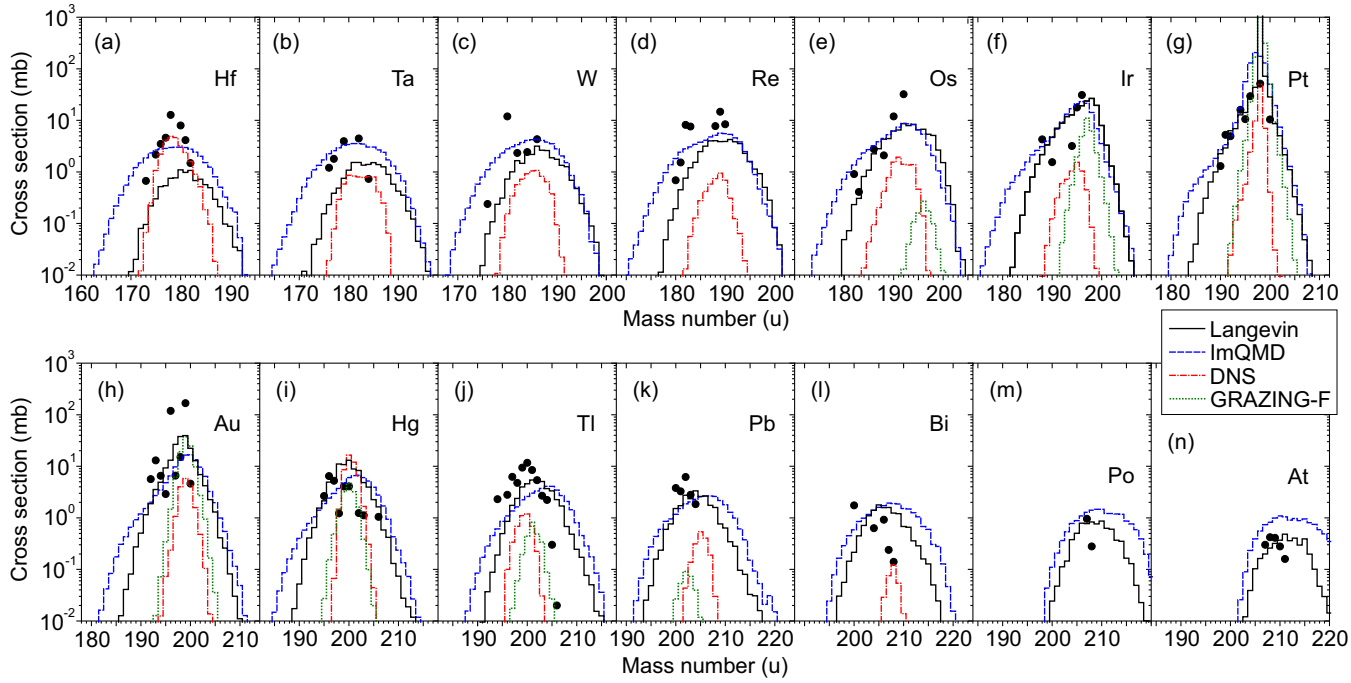

FIG. 4. Isotopic distributions of the final TLFs obtained in the ^{136}Xe + ^{198}Pt reaction at $E_{\text{c.m.}} = 450$ MeV. The circles indicate the experimental data for elements from Hf ($Z = 72$) to At ($Z = 85$) [42]. Calculation results obtained within the present dynamical model are shown by solid histograms. Calculation results of ImQMD, DNS, and GRAZING-F approaches taken from Ref. [42] are also shown by the dashed, dash-dotted, and dotted histograms, respectively.

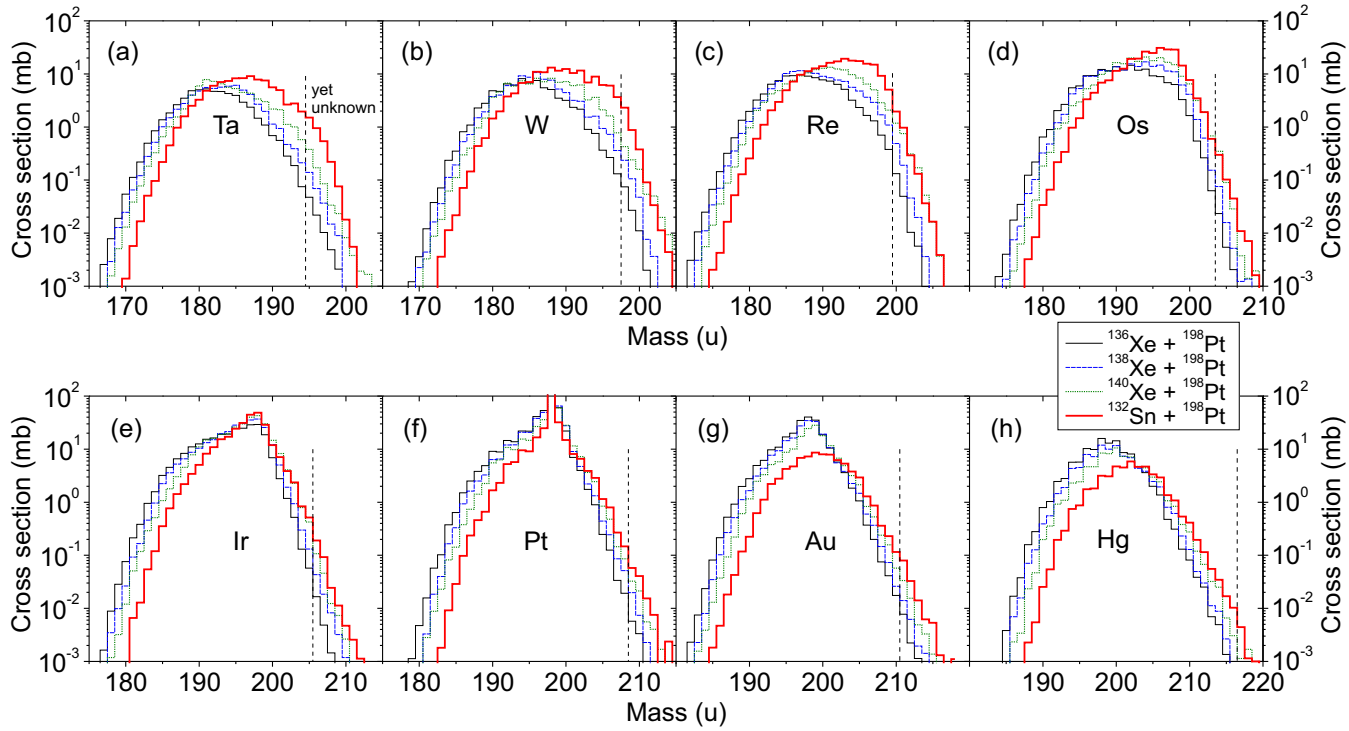

FIG. 5. Calculated final isotopic distributions of elements from Ta ($Z = 73$) to Hg ($Z = 80$) obtained in MNT reactions induced by radioactive-ion beams on the ^{198}Pt target. The solid, dashed, dotted, and thick histograms indicate cross sections for the reactions ^{136}Xe + ^{198}Pt ($E_{\text{c.m.}} = 498$ MeV), ^{138}Xe + ^{198}Pt ($E_{\text{c.m.}} = 496$ MeV), ^{140}Xe + ^{198}Pt ($E_{\text{c.m.}} = 495$ MeV), and ^{132}Sn + ^{198}Pt ($E_{\text{c.m.}} = 460$ MeV), respectively. Vertical dashed lines show the boundaries of the regions of yet unknown nuclei.

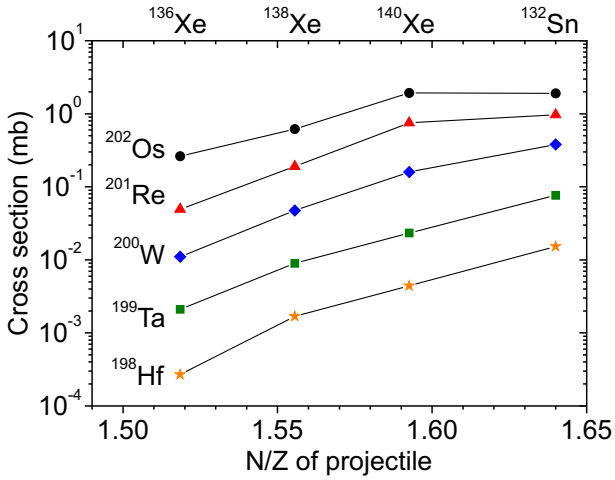

FIG. 6. The production cross sections of isotopes from hafnium to osmium ($Z = 72$–76) with the neutron number $N = 126$ obtained in the reactions ^{136,138,140}Xe + ^{198}Pt and ^{132}Sn + ^{198}Pt as a function of the N/Z ratio of the projectile. The projectiles are indicated at the top of the figure.

cross sections. In particular, the so far unknown neutron-enriched isotopes ^{195}Ta, ^{197}W, and ^{200}Re are predicted to be produced with cross sections exceeding the 1-mb level in the ^{132}Sn + ^{198}Pt reaction.

The cross sections of neutron-enriched nuclides with the magic number $N = 126$ calculated in the MNT reactions under study plotted over the N/Z ratio of projectile are shown in Fig. 6. An exponential increase of the cross-section values is found for nuclides with greater neutron excess.

Similar qualitative results were obtained within the DNS model and its modification for the same and similar reactions [19,20]. However, the cross sections obtained in those works decrease much steeper with increasing the number of transferred nucleons.

C. Production yields of neutron-enriched nuclides with $N = 126$

The production rate I or the yield of a particular product obtained in a nuclear reaction is proportional not only to the cross section σ but also to the intensity of the beam I_0:

$$I = \rho l \sigma I_0, \tag{3}$$

where ρl is the number of atoms in the target per unit of surface area. Since the quantity ρl is the characteristic of the target, we can eliminate its contribution from Eq. (3) and consider the quantity σI_0 to characterize the yield I. Such σI_0 values calculated for the case of the yet unknown nuclides ^{201}Re and ^{200}W with $N = 126$ are plotted over the N/Z ratio of the projectile in Fig. 7. The available intensities of ^{132}Sn and ^{136,138,140}Xe RIBs [21–24] shown in Fig. 7 were used in the calculations.

Depending on the RIB facility, the σI_0 values behave differently with increasing the N/Z ratio of the projectile. However, according to calculations, the highest production rates could be obtained at the SPIRAL2 and ISOLDE facilities.

An increase in the yields of ^{200}W with the growing N/Z ratio of the projectile is observed in the case of the RIB intensities available at ISOLDE [see Fig. 7(b)]. Similar results can be obtained for other, yet unknown, neutron-enriched nuclides with $N = 126$, since their cross sections also increase with increasing the N/Z ratio of the projectile (Fig. 6).

The production rates obtained in the RIB-induced MNT reactions are nearly an order of magnitude lower than those provided by the currently available beams of stable projectiles. Therefore, MNT reactions induced by neutron-rich RIBs remain an impractical method so far. However, technologies for producing RIBs are developing: existing facilities are being modernized, and new larger ones, like EURISOL, FAIR, RAON, etc., are being designed and built. Therefore, in the near future, RIB facilities may provide powerful beams, which can lead to the experimental investigation of neutron-enriched heavy nuclei in MNT reactions induced by RIBs.

IV. CONCLUSIONS AND OUTLOOK

In this paper, the multinucleon transfer processes in the reactions ^{132}Sn + ^{198}Pt and ^{136,138,140}Xe + ^{198}Pt are analyzed within the dynamical model based on the Langevin

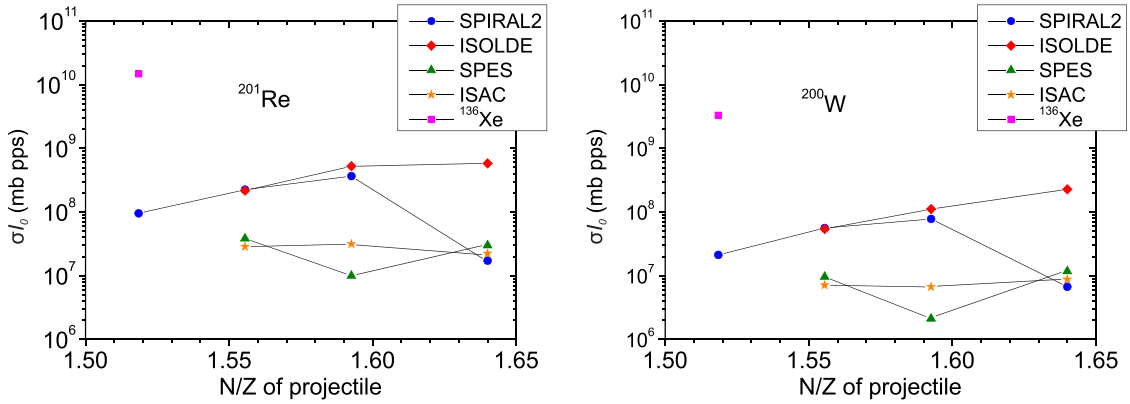

FIG. 7. Calculated values of σI_0 for yet unknown neutron-enriched isotopes with the magic number $N = 126$, ^{201}Re (a) and ^{200}W (b), obtained in the MNT reactions ^{136,138,140}Xe + ^{198}Pt and ^{132}Sn + ^{198}Pt.

equations. The model provides reasonable agreement with the experimental isotopic distributions of the reaction products obtained in the MNT reaction ^{136}Xe + ^{198}Pt at $E_{\text{c.m.}} = 450$ MeV.

The use of more neutron-rich projectiles in reaction with the ^{198}Pt target leads to higher cross sections of neutron-enriched nuclides with the neutron number $N = 126$ due to the N/Z-equilibration process. Analysis of production rates in these reactions taking into account current RIB intensities available at the SPIRAL2, ISOLDE, SPES, and ISAC facilities has shown that the yields of heavy neutron-enriched nuclides with $N = 126$ increase with increasing neutron excess of the projectile.

ACKNOWLEDGMENTS

This work was funded by the Ministry of Science and Higher Education of the Russian Federation through Grant No. 075-10-2020-117. This research was also funded by the Science Committee of the Ministry of Science and Higher Education of the Republic of Kazakhstan (Grant No. AP19679767).

[1] V. Zagrebaev and W. Greiner, J. Phys. G: Nucl. Part. Phys. **35**, 125103 (2008).
[2] A. V. Karpov and V. V. Saiko, Phys. Rev. C **96**, 024618 (2017).
[3] G. G. Adamian, N. V. Antonenko, A. Diaz-Torres, and S. Heinz, Eur. Phys. J. A **56**, 47 (2020).
[4] A. V. Yeremin, S. Heinz, H. M. Devaraja, and A. G. Popeko, Phys. Part. Nucl. Lett. **19**, 693 (2022).
[5] S. Ayik, M. Arik, O. Yilmaz, B. Yilmaz, and A. S. Umar, Phys. Rev. C **107**, 014609 (2023).
[6] A. G. Artukh, G. F. Gridnev, V. L. Mikheev, and V. V. Volkov, Nucl. Phys. A **137**, 348 (1969).
[7] A. G. Artukh, V. V. Avdeichikov, G. F. Gridnev, V. L. Mikheev, V. V. Volkov, and J. Wilczynski, Nucl. Phys. A **176**, 284 (1971).
[8] K. Becker *et al.*, Nucl. Phys. A **522**, 557 (1991).
[9] K.-L. Gippert *et al.*, Nucl. Phys. A **453**, 1 (1986).
[10] K. J. Moody *et al.*, Z. Phys. A **328**, 417 (1987).
[11] J. Kurcewicz *et al.*, Phys. Lett. B **717**, 371 (2012).
[12] Y. X. Watanabe, Y. H. Kim, S. C. Jeong, Y. Hirayama, N. Imai, H. Ishiyama *et al.*, Phys. Rev. Lett. **115**, 172503 (2015).
[13] C. H. Dasso, G. Pollarolo, and A. Winther, Phys. Rev. Lett. **73**, 1907 (1994).
[14] H. Freiesleben and J. V. Kratz, Phys. Rep. **106**, 1 (1984).
[15] W. Krolas *et al.*, Nucl. Phys. A **832**, 170 (2010).
[16] R. Planeta *et al.*, Phys. Rev. C **38**, 195 (1988).
[17] A. S. Umar, C. Simenel, and W. Ye, Phys. Rev. C **96**, 024625 (2017).
[18] V. Saiko and A. Karpov, Eur. Phys. J. Web Conf. **223**, 01055 (2019).
[19] L. Zhu, J. Su, W.-J. Xie, and F.-S. Zhang, Phys. Lett. B **767**, 437 (2017).
[20] Z. Liao, L. Zhu, J. Su, and C. Li, Phys. Rev. C **107**, 014614 (2023).
[21] Available beams at the SPIRAL2, https://u.ganil-spiral2.eu/chartbeams.
[22] The ISOLDE yield database, https://isoyields2.web.cern.ch.
[23] Available beams at the SPES, https://web.infn.it/spes/index.php/news/spes-beam-tables.
[24] The ISAC yield database, https://mis.triumf.ca/science/planning/yield/beam.
[25] Y. Abe, S. Ayik, P.-G. Reinhard, and E. Suraud, Phys. Rep. **275**, 49 (1996).
[26] P. Fröbrich and I. I. Gontchar, Phys. Rep. **292**, 131 (1998).
[27] A. V. Karpov and G. D. Adeev, Eur. Phys. J. A **14**, 169 (2002).
[28] G. D. Adeev, A. V. Karpov, P. N. Nadtochy, and D. V. Vanin, Phys. Part. Nucl. **36**, 378 (2005).
[29] V. Zagrebaev and W. Greiner, J. Phys. G: Nucl. Part. Phys. **31**, 825 (2005).
[30] Y. Aritomo, Nucl. Phys. A **780**, 222 (2006).
[31] A. J. Sierk, Phys. Rev. C **96**, 034603 (2017).
[32] V. V. Saiko and A. V. Karpov, Phys. Rev. C **99**, 014613 (2019).
[33] J. Maruhn and W. Greiner, Z. Phys. **251**, 431 (1972).
[34] V. Zagrebaev, A. Karpov, Y. Aritomo, M. Naumenko, and W. Greiner, Phys. Part. Nucl. **38**, 469 (2007).
[35] A. V. Karpov, A. S. Denikin, A. P. Alekseev, V. I. Zagrebaev, V. A. Rachkov, M. A. Naumenko, and V. V. Saiko, Phys. At. Nucl. **79**, 749 (2016).
[36] K. T. R. Davies, A. J. Sierk, and J. R. Nix, Phys. Rev. C **13**, 2385 (1976).
[37] A. J. Sierk and J. R. Nix, Phys. Rev. C **21**, 982 (1980).
[38] V. I. Zagrebaev, A. P. Alekseev, A. S. Denikin, A. V. Karpov, M. A. Naumenko, V. A. Rachkov, V. V. Samarin, and V. V. Saiko, NRV web knowledge base on low-energy nuclear physics, http://nrv.jinr.ru.
[39] K.-H. Schmidt, B. Jurado, C. Amouroux, and C. Schmitt, Nucl. Data Sheets **131**(Suppl. C), 107 (2016).
[40] M. G. Itkis and A. Ya. Rusanov, Phys. Part. Nucl. **29**, 160 (1998).
[41] R. Bass, *Lecture Notes in Physics* (Springer, Berlin, 1980), Vol. 117.
[42] V. V. Desai, W. Loveland, R. Yanez, G. Lane, S. Zhu, A. D. Ayangekaa, J. P. Greene, F. G. Kondev, R. V. F. Janssens, and P. A. Copp, Eur. Phys. J. A **56**, 150 (2020).
[43] C. Li, X. Xu, J. Li, G. Zhang, B. Li, C. A. T. Sokhna, Z. Ge, F. Zhang, P. Wen, and F.-S. Zhang, Phys. Rev. C **99**, 024602 (2019).
[44] R. Yanez and W. Loveland, Phys. Rev. C **91**, 044608 (2015).